PAPER

Voltage-induced high-speed DW motion in a synthetic antiferromagnet

IOP Publishing Journal of Physics D: Applied Physics
J. Phys. D: Appl. Phys. **52** (2019) 495001 (7pp) https://doi.org/10.1088/1361-6463/ab3fc9

Voltage-induced high-speed DW motion in a synthetic antiferromagnet

Lulu Chen[1], Maokang Shen[1], Yingying Peng, Xinyu Liu, Wei Luo, Xiaofei Yang, Long You and Yue Zhang[2]

School of Optical and Electronic Information, Huazhong University of Science and Technology, Wuhan, 430074, People's Republic of China

E-mail: yue-zhang@hust.edu.cn (Y Zhang)

Received 25 June 2019, revised 15 August 2019
Accepted for publication 30 August 2019
Published 18 September 2019

Abstract

Voltage-induced motion of a magnetic domain wall (DW) has potential in developing novel devices with ultralow dissipation. However, the speed for the voltage-induced DW motion (VIDWM) in a single ferromagnetic layer is usually very low. In this work, we proposed VIDWM with high speed in a synthetic antiferromaget (SAF). In the medium with a small damping coefficient, the velocity for the coupled DWs in the SAF is significantly higher than its counterpart in a single ferromagnetic layer. Strong interlayer antiferromagnetic exchange coupling plays a critical role for the high DW velocity since it inhibits the tilting of DW plane with Dzyaloshinskii–Moriya interaction. On the other hand, in the material with a large damping coefficient, the Walker breakdown of DW motion is also inhibited due to the stabilization of moment orientation under a strong interlayer antiferromagnetic coupling. In theory, the voltage-induced gradient of magnetic anisotropy is proved to be equal to an effective magnetic field that drives DW.

Keywords: domain wall, voltage-induced domain wall motion, synthetic antiferromagnet, gradient of magnetic anisotropy

(Some figures may appear in colour only in the online journal)

Motion of magnetic domain walls (DWs) exhibits significant potential in development of wide novel magneto electronic devices, such as racetrack memory, magnetic logic devices, and spin memristors for mimicking synapse in artificial neural network [1–4]. Voltage-induced DW motion (VIDWM) has outstanding advantage for low dissipation, and it attracts wide research attention [5–9]. Electric-field control of DW motion was initially observed only in the creep region and was found to diminish at high DW velocities due to the modulation of activation energy barrier by gate voltage [6, 9, 10]. Lin *et al* described the electric field induced effective magnetic field and experimentally demonstrated it to be a universal effect from the creep to the flow region [7]. However, the electric field is inefficient for high DW velocities due to the Walker breakdown under a high electric field [5, 7]. In theory, the DW velocity under sloped electric field is several m/s [5]. In experiment, the DW velocity may be smaller due to extrinsic pinning effect from defects. Very recently, Ma *et al* reported VIDWM with a velocity at the magnitude of cm/s driven by a sloped electric field [11]. To further accelerate the VIDWM in an FM track, complicated fabrication technology seems necessary [12].

A high DW velocity is expectable for VIDWM in a synthetic antiferromagnet (SAF), in which a high velocity (750 m s^{-1} or higher) of current-induced DW motion has been reported [13, 14]. This ultrahigh velocity is mainly attributed to strong antiferromagnetic exchange coupling between two FM layers and the interfacial Dzyaloshinskii–Moriya interaction (DMI) between a heavy metal layer and a ferromagnetic (FM) layer [13]. Very recently, voltage-induced motion of coupled skyrmions in an SAF at an ultrahigh velocity was proposed [15]. Nevertheless, the device based on DW motion seems easier in technique. In this work, VIDWM in the SAF is studied numerically and clear increase in DW velocity and inhibition of Walker breakdown has been observed and explained in theory.

[1] These authors contributed equally to this work.
[2] Author to whom any correspondence should be addressed.

The schematic of VIDWM in the SAF is shown in figure 1. In principle, the VIDWM is based on manipulation of magnetic anisotropy constant under an external voltage. In application, two routes can be exploited. One is based on the multiferroic behavior with the combination of converse piezoelectric effect and magnetostriction effect (figure 1(b)) [5]. The other is originated from the variation of charge state at the metal/insulator interface under an external electric field (figure 1(c)) [6–10]. In either case, a wedge-shaped piezoelectric substrate or insulator layer is necessary for inducing an electric field strength (E) increasing from one end to the other one under a voltage. This sloped E gives rise to spatial variation of magnetic anisotropy energy, and the DW in the FM layer moves towards the end with a lower anisotropy energy [5, 16]. In the SAF, the DWs in the upper and lower layer move together when the interlayer exchange coupling is strong enough.

The object-oriented micromagnetic framework (OOMMF) software with the code of interfacial DMI was exploited to do the micromagnetic simulation [17]. The model is a cuboid-shaped track of SAF multilayer with perpendicular magnetic anisotropy (PMA). The parameters are as follows. The length and width of the track are 600 nm and 100 nm, respectively. The thickness of the lower layer, the upper layer, and the interlayer is 0.6 nm. The cell dimension is 2 nm × 1 nm × 0.6 nm. The saturation magnetization (M_S) is 5.8×10^5 A m^{-1} for Pt/Co. The damping coefficient α is from 0.03 to 0.2 for different composition. For example, CoFeB has a small α, while Pt/Co has a large one [18, 19]. For simplicity, while studying the influence of α in VIDWM, the difference of other magnetic parameters, such as M_S, is not considered. The DMI constant (D) varies between 0 mJ m^{-2} and −3 mJ m^{-2}. The exchange stiffness constant (A) is 1.5×10^{-11} J m^{-1}. The interlayer Ruderman–Kittel–Kasuya–Yosida (RKKY) exchange coupling parameters (J_{ex}) between two FM layers is between 0 J m^{-2} and -1×10^{-3} J m^{-2}. To study the variation of magnetic anisotropy constant (K) in the track, a Cartesian coordinate system is set up with the origin located at the left track end and the x axis pointing to right. We assume K varies as a linear function of x, $K = ax + b$. Here a is the gradient of anisotropy constant, between 0 GJ m^{-4} and −2800 GJ m^{-4}. At a small a (−200 GJ m^{-4}, −400 GJ m^{-4}, and −600 GJ m^{-4}), b, the anisotropy constant at the left track end, is fixed as 8×10^5 J m^{-3}. While at a higher a (−800 GJ m^{-4} and higher), to ensure the PMA for the whole or most part of track, the anisotropy constant in the middle of track (K ($x = 300$ nm)) is fixed as 1.2×10^6 J m^{-3}. The DW motion in a single FM layer was also simulated for comparison. At first, we consider the VIDWM at a high velocity in the track with a low α at small a. Afterwards, the VIDWM for a high damping is studied at a higher a.

Initially, the DW is generated in the middle of track ($x = 300$ nm) with a small α ($\alpha = 0.03$). Because of the negative D, the DW exhibits Néel-type structure with left-handed chirality. At initio, the azimuthal angles for the moment in the central of DW in the lower and upper layer ($\varphi_{L(U)}$ with L(U) representing lower (upper)) are 180° and 360°, respectively. In general, the DW with PMA prefers a Bloch-type structure to lower the shape anisotropy energy of DW. However, under strong DMI, the Néel-type structure is more stable in total energy at the cost of increasing shape anisotropy energy [20]. After the gradient of K is applied on the track, the DW starts to move towards the end with smaller K. In the single FM layer, the DW velocity is smaller than 200 m s^{-1} and the DW plane tilts when the gradient of K reaches −600 GJ m^{-4} due to strong DMI [21–24]. However, in the SAF, the DWs move clearly faster and the DW tilting is inhibited by the interlayer RKKY interaction (figures 1(b)–(d)).

The instantaneous velocity (v) of DW is derived quantitatively by differentiating q with respect to t. It is noticed the DW moves at an almost constant velocity when a is as small as −200 GJ m^{-4} in either single FM layer or SAF, but it moves at an ever-increasing speed when a becomes −600 GJ m^{-4} (figures 2(c), (f) and (i)). This accelerated motion is special for the VIDWM [16]. In general, the DW velocity is strictly related to temporal φ, and it becomes stable when the φ reaches a constant value. In the single FM layer, the φ keeps increasing in the process of DW motion for a large a (figure 2(a)), which is accompanied with an accelerated DW motion. In the SAF, the changing of φ with time is depressed significantly. On the other hand, the $\varphi_{L(U)}$ is also much closer to 180°(360°) for a stronger interlayer RKKY coupling. Nevertheless, the DW velocity still keeps increasing even though a is as large as −600 GJ m^{-4}. This indicates that strong RKKY coupling contributes to the accelerated DW motion with stabilized DW structure.

The above observation can be further confirmed from the influence of DMI on VIDWM. In racetrack memory of an FM track, DMI is a double-edge sword for application: a moderate DMI offers a torque that contributes to the driving force of DW motion [25], but a strong DMI tilts the DW plane that reduces the DW motion [26]. This can be reflected from the nonmonotonous relationship between average DW velocity (v_a) or φ and D (figure 3). The v_a in this paper is calculated based on DW motion between $x = 350$ nm and $x = 400$ nm. In a single FM layer, because the effective field of DMI is along the x direction, strong DMI torque is acted on DW magnetization only if φ deviates from the initial 0° or 180° under external driving force [25]. In other words, deviation from initial Néel-type DW structure is the prerequisite to a strong DMI torque that drives DW. This is consistent with the results for the single FM layer in figures 3(a) and (b). For the VIDWM in SAF with a strong RKKY coupling, if only DMI is not too weak, the $\varphi_{L(U)}$ is closer to 180°(360°), yet the DW moves at an even much higher velocity (figures 3(c)–(f)). This proves that instead of DMI the RKKY coupling contributes mainly to the high-speed VIDWM in SAF.

The results shown above are for medium with a very low damping coefficient ($\alpha = 0.03$). In this case, the DW plane in a single FM layer with strong DMI may tilt soon after it starts moving [21]. In the following, we consider the VIDWM for a large damping coefficient ($\alpha = 0.2$). We have simulated the DW motion in a single layer and SAF with different DMI under a large a (figures 4(a) and (b)). In a single layer with $D = -0.05$ mJ m^{-2}, when a is lower than −1500 GJ m^{-4}, the DW in the SAF moves a little faster than that in the single FM layer. When a is −1500 GJ m^{-4} or higher, Walker breakdown

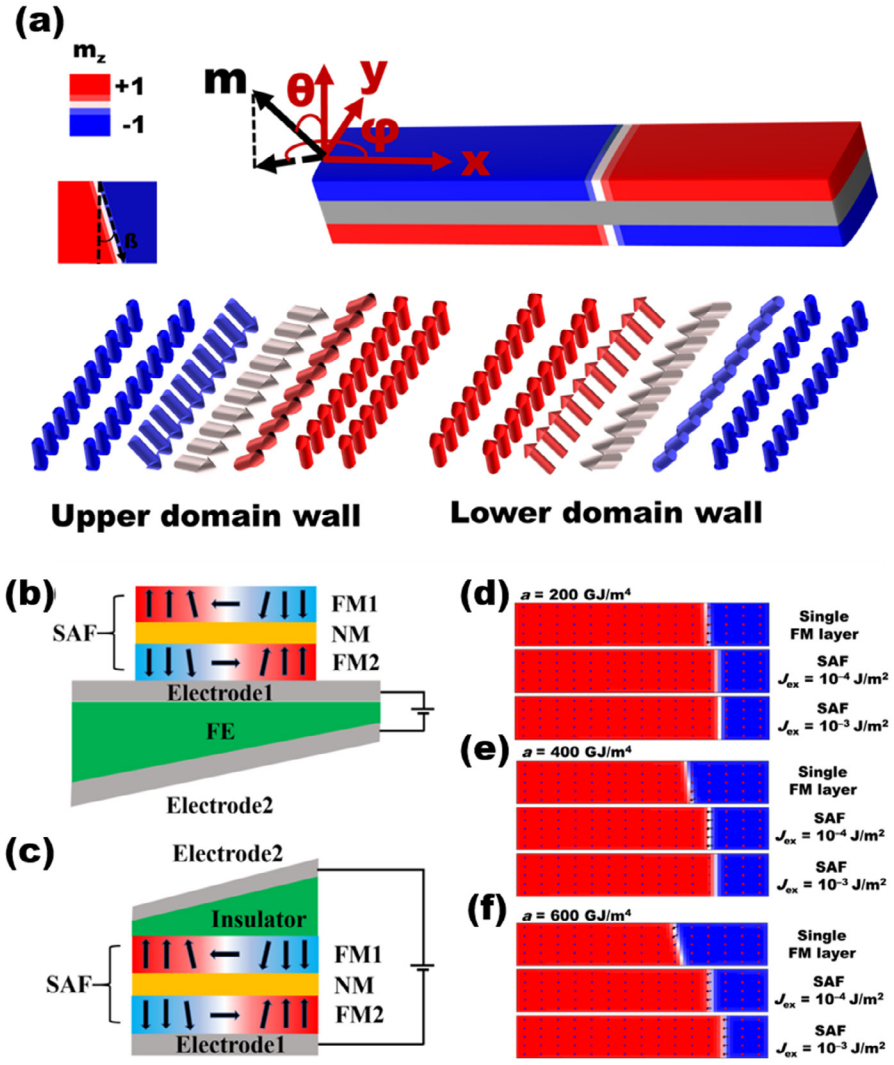

Figure 1. Schematic of the coupled DW system in an SAF with negative DMI constant (a) and VIDWM based on multiferroic behavior (b) and manipulation of charge state at metal/insulator interface (c). (d)–(f) DW motion under different voltage-induced gradient of magnetic anisotropy energy in a single FM layer and in the SAFs with different interlayer exchange coupling. The Cartesian coordinate system, the unit vector for the direction of magnetization (m), the polar angle (θ), the azimuthal angle (φ), and the tilting angle of DW plane (β) are all illustrated in (a).

occurs in the single FM layer but it is not observed in the SAF with $J_{ex} = -10^{-3}$ J m^{-2} even when a is as high as -2800 GJ m^{-4} (figure 4(a)). In the single layer and the SAF with stronger DMI ($D = -1.2$ mJ m^{-2}), the Walker breakdown is depressed, which is consistent with the theoretical prediction [21, 27]. On the other hand, the v_a in both single FM layer and SAF has little difference (figure 4(b)), indicating a large gradient of magnetic anisotropy constants dominates the DW motion no matter what the structure is. In addition to DMI, the tilting angle of DW plane (β) is also relevant to the damping coefficient. In this work, β is measured for the DW at $x = 400$ nm. In the single FM layer, β decreases drastically with α increasing from 0.03 to 0.2. Correspondingly, the v_a of SAF is clearly higher than that in the single FM layer when α is smaller than 0.1 (figure 4(c)). On the other hand, the tilting of DW in an SAF plane is effectively inhibited when J_{ex} is -1×10^{-4} J m^{-2} or larger, which is accompanied with increasing DW velocity. At a weaker RKKY coupling, the DW planes in the two layers of SAF tilt towards opposite directions, leading to weak interlayer coupling and slow DW motion (figure 4(d)).

In theory, DW motion driven by the gradient of K can be depicted by the collective coordinate method (CCM). For studying VIDWM by CCM, one needs to pay attention to the DW width (Δ) that is described as:

$$\Delta = \sqrt{A/\left(ax + b - \frac{1}{2}\mu_0 M_S^2\right)}. \quad (1)$$

Clearly, Δ is a function of x at different a (figure 5(a)). The DW is significantly widened when it moves towards the right track end with a lower anisotropy constant. If this variation of Δ is considered in CCM, the calculation is rather complicated [16]. For simplification, the DW width is approximately taken as a constant for small a (-200 GJ m^{-4}, -400 GJ m^{-4}, and -600 GJ m^{-4}). In this case, the variation of Δ is relatively small. As illustrated in figure 1(a), the collective

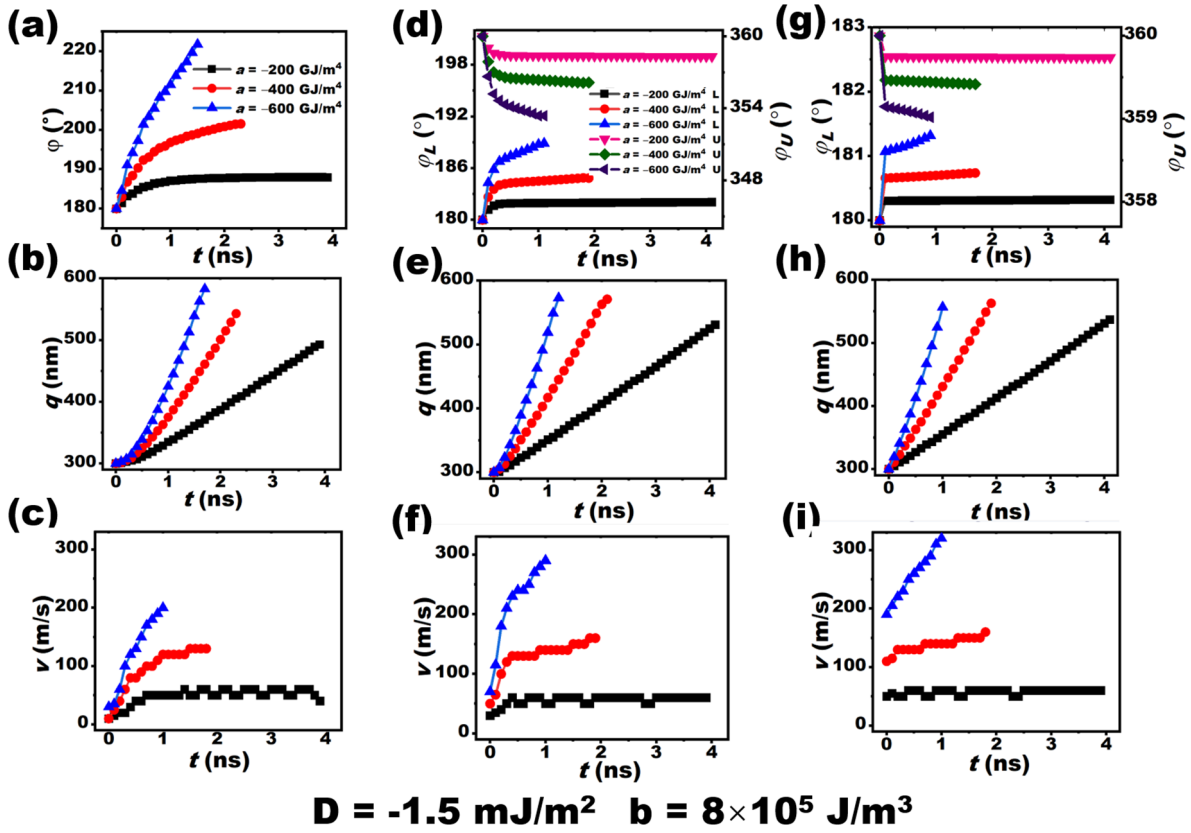

Figure 2. Azimuthal angle (φ), central position of DW (q), and instantaneous velocity (v) as a function of time (t) at different gradient of magnetic anisotropy energy in a single FM layer (a)–(c) and in the SAF with $J_{ex} = -1 \times 10^{-4}$ J m^{-2} (d)–(f) and $J_{ex} = -1 \times 10^{-3}$ J m^{-2} (g)–(i). The φ_L and φ_U represent the azimuthal angle for the DW magnetization in the central of DW at the lower and upper layer, respectively. D and b are fixed as -1.5 mJ m^{-2} and 8×10^5 J m^{-3}, respectively.

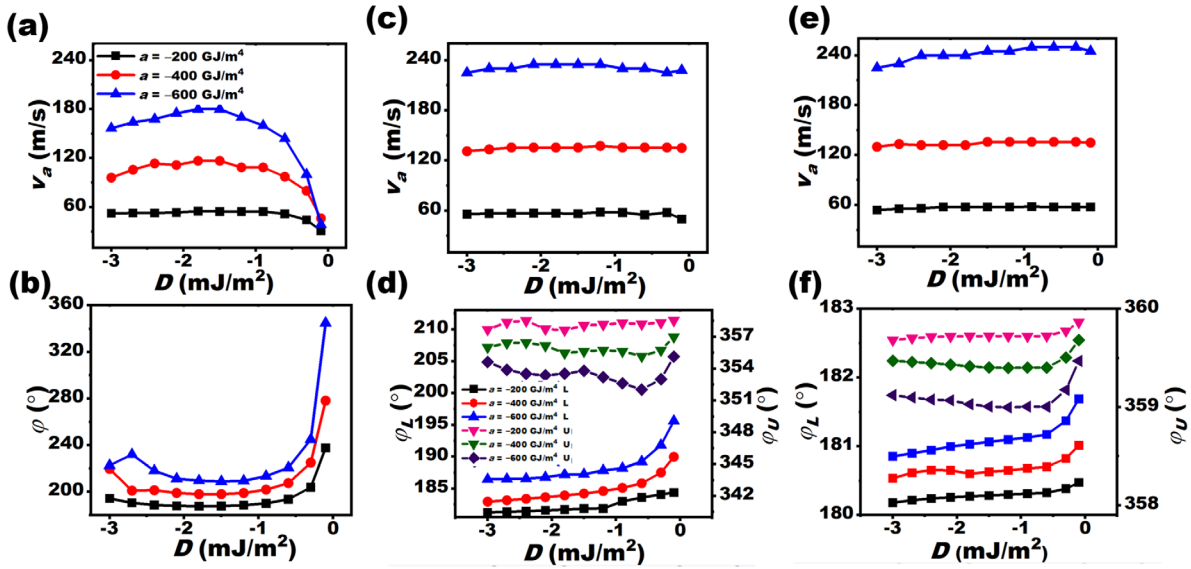

Figure 3. Average DW velocity (v_a) and azimuthal angle ($\varphi_{L(U)}$) as a function of DMI constant (D) under different gradient of magnetic anisotropy energy in a single FM layer (a), (b) and in the SAF with $J_{ex} = -1 \times 10^{-4}$ J m^{-2} (c), (d) and $J_{ex} = -1 \times 10^{-3}$ J m^{-2} (e), (f).

coordinates, including the position, the azimuthal angle, and the polar angle of the moment in the central of DW, are labeled as $q_{L(U)}$, $\varphi_{L(U)}$, and $\theta_{L(U)}$, respectively. In a spherical coordinate system, the unit vector for the direction of magnetization is $\vec{m}_{L(U)} = (\sin\theta_{L(U)}\cos\varphi_{L(U)}, \sin\theta_{L(U)}\sin\varphi_{L(U)}, \cos\theta_{L(U)})$, and the ansatz is expressed as [13]:

$$\theta_L = 2\arctan\{\exp[(x - q(t))/\Delta]\}, \quad \varphi_L = \varphi_L(t), \quad (2)$$

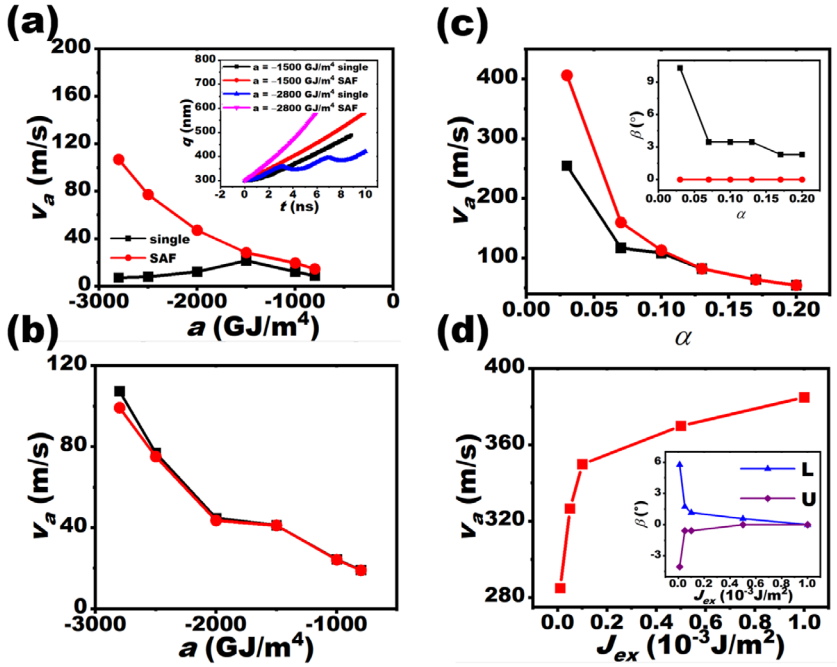

Figure 4. Average DW velocity (v_a) as a function of gradient of magnetic anisotropy constant (a) in a single FM layer and SAF for (a) $D = -0.05$ mJ m^{-2} and (b) $D = -1.2$ mJ m^{-2}. The inset in (a) shows time dependence of central position of DW (q); v_a as a function of damping coefficient (α) in the single FM layer and SAF (c) and RKKY interlayer exchange coupling constant (J_{ex}) (d). (The J_{ex} in (a)–(c) is -1×10^{-3} J m^{-2}; the D and a in (c) and (d) are -1.2 mJ m^{-2} and -2000 GJ m^{-4}, respectively. The insets in (c) and (d) depict the tilting angle for the DW plane in the single FM layer and SAF as a function of α and J_{ex}, respectively.)

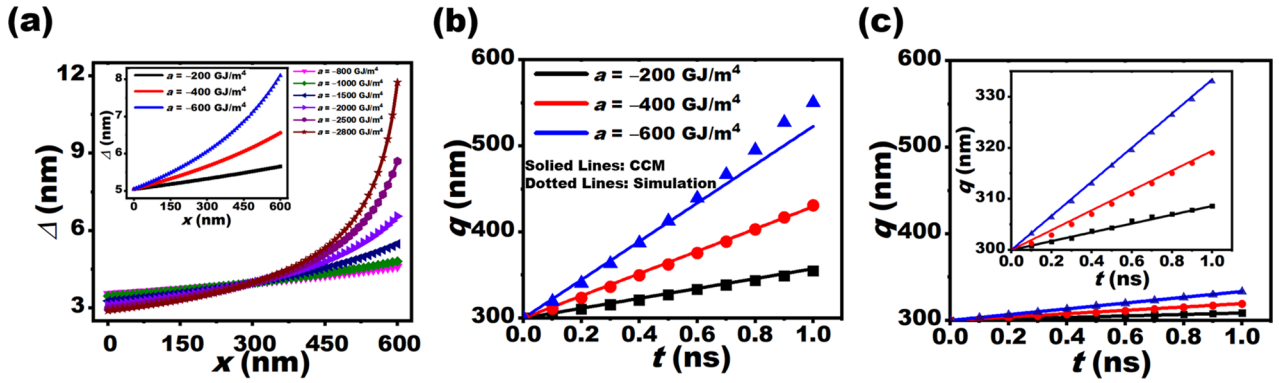

Figure 5. Variation of DW width (Δ) with x at different a (a). (The inset shows the Δ as a function of x as a varying from -200 GJ m^{-4} to -600 GJ m^{-4}.) Central position (q) as a function of time (t) for the damping coefficient $\alpha = 0.03$ (b) and $\alpha = 0.2$ (c). (The solid lines are the numerical solution of CCM and the dotted lines are the result of micromagnetic simulation.)

and

$$\theta_U = 2\arctan\{\exp[(x - q(t))/\Delta]\} + \pi, \quad \varphi_U = \varphi_U(t). \tag{3}$$

Here Δ is the DW width that is approximately written as:

$$\Delta = \sqrt{A/\left(K_0 - \frac{1}{2}\mu_0 M_S^2\right)}. \tag{4}$$

Here K_0 means the magnetic anisotropy constant at the initial position of DW, i.e. at $x = 300$ nm.

The DW dynamics is depicted quantitatively through the Gilbert equation:

$$\frac{d\vec{m}_i}{dt} = -\gamma\vec{m}_i \times (\vec{H}_{eff})_i + \alpha\vec{m}_i \times \frac{d\vec{m}_i}{dt}, \quad (i = L, U). \tag{5}$$

Here γ is the absolute value of gyromagnetic ratio of an electron. $\vec{H}_{eff}$ is the effective magnetic field that is related to the free energy density w as:

$$(\vec{H}_{eff})_i = -\frac{1}{\mu_0 M_s}\frac{\delta w_i}{\delta \vec{m}_i}, \tag{6}$$

and

$$\begin{aligned} w_i = {} & \tfrac{A}{\Delta^2}\sin^2\theta_i + \left(K_0 - \tfrac{1}{2}\mu_0 M_S^2\right)\sin^2\theta_i + \tfrac{1}{2}\mu_0 N_x M_S^2 \sin^2\theta_i \cos^2\varphi_i \\ & + \tfrac{D\sin\theta_i\cos\varphi_i}{\Delta} - \tfrac{J_{ex}}{t_s}[\sin\theta_L \sin\theta_U \cos(\varphi_L - \varphi_U) + \cos\theta_L \cos\theta_U] \\ & - \mu_0 M_S (H_z)_i \cos\theta_i. \end{aligned} \tag{7}$$

The N_x is the demagnetizing factor in the x direction [16]. $(H_z)_i$ represents the effective magnetic field for the gradient

of magnetic anisotropy. The absolute value of H_z of the two layers are the same [16]:

$$H_z = \frac{1}{2M_S}\frac{d\sigma}{dx} = \frac{a\sqrt{A}}{M_S}(ax+b)^{-\frac{1}{2}}. \quad (8)$$

σ is the DW energy per unit area, and the signs of H_z for the two layers are opposite due to the opposite transition of magnetization in the two layers when two coupled DWs move in the same direction. Equations (6)–(8) were put into equation (5) and the group of Thiele equations were derived after the integration for the whole track:

$$\frac{2\alpha}{\Delta}\dot{q} + \dot{\varphi}_L - \dot{\varphi}_U = -\frac{2\gamma\Delta a}{M_s}; \quad (9)$$

$$\frac{1}{\Delta}\dot{q} - \alpha\dot{\varphi}_L = -\frac{\gamma\pi D\sin\varphi_L}{2\Delta M_S} - \frac{\gamma\mu_0 N_x M_S \sin 2\varphi_L}{2} + \frac{\gamma J_{ex}}{M_S t_s}\sin(\varphi_U - \varphi_L); \quad (10)$$

$$-\frac{1}{\Delta}\dot{q} - \alpha\dot{\varphi}_U = -\frac{\gamma\pi D\sin\varphi_U}{2\Delta M_S} + \frac{\gamma\mu_0 N_x M_S \sin 2\varphi_U}{2} + \frac{\gamma J_{ex}}{M_S t_s}\sin(\varphi_L - \varphi_U). \quad (11)$$

The group of Thiele equations were resolved numerically with the initial condition $q = 300\,\text{nm}$, $\varphi_L = 180°$, and $\varphi_U = 360°$. The numerical solution is close to that obtained from the simulation (figures 5(b) and (c)). The small deviation in figure 5(b) for $a = -600$ GJ m^{-4} may come from the approximation for the constant DW width. Under this condition, the DW is able to move quickly to approach the right end of track where the DW is widened obviously.

Finally, the electric field strength (E) for inducing the gradient of anisotropy constant is estimated. Linear variation of surface anisotropy constant (ΔK_s) with E has been reported in CoFeB/MgO ultrathin film with PMA, i.e. $\Delta K_s = \beta E$. Here β is magnetoelectric coefficient and around 100 fJ Vm^{-1} for CoFeB/MgO [28]. Assuming a 1 nm thick CoFeB and zero E at the left end of track, we estimated the variation of E in the nanotrack with small gradient of anisotropy ($a = -200$ GJ m^{-4}, -400 GJ m^{-4}, and -600 GJ m^{-4}). The maximum E throughout the track increases from 1.2 V nm^{-1} to 3.6 V nm^{-1} with increasing a from -200 GJ m^{-4} to -600 GJ m^{-4}, respectively. The electric field with this strength is reasonable in experiment.

In summary, a high-speed VIDWM in an SAF is predicted based on an electric-field-induced gradient of magnetic anisotropy. When the damping coefficient of the medium is low, the velocity for the coupled DWs in the SAF is clearly higher than its counterpart in a single FM layer due to the inhabitation of the DMI-induced tilting of DW plane by the interlayer RKKY exchange coupling. On the other hand, strong RKKY coupling also plays a critical role for depressing the Walker breakdown in a medium with a high damping coefficient. In theory, the gradient of magnetic anisotropy is proved to be equal to an effective magnetic field that drives DW. In application, the VIDWM may be realized based on multiferroic behaviors [29, 30] or voltage-induced variation of charge state at the metal/insulator interface [31]. In the latter case, the electric-field strength is estimated to be at the magnitude of several V/nm, which is reasonable in experiment. It is interesting to note that the VIDWM in a wedged FM film has been successfully realized in experiment very recently [11]. On the other hand, the experimental work about current-induced DW motion in an SAF with an ultrahigh velocity has also been reported [13]. Therefore, our proposal about VIDWM in an SAF seems a realistic route for improving the velocity of DW motion driven by electric field, and the further experimental investigation is much anticipated.

Acknowledgments

This work was supported by the National Natural Science Foundation of China (Grant No. 11574096) and Huazhong University of Science and Technology (No. 2017KFYXJJ037).

ORCID iDs

Yue Zhang https://orcid.org/0000-0002-1994-3071

References

[1] Stuart S, Parkin P, Hayashi M and Thomas L 2008 *Science* **320** 190
[2] Allwood D A, Xiong G, Faulkner C C, Atkinson D, Petit D and Cowburn R P 2005 *Science* **309** 1688
[3] Locatelli N, Cros V and Grollier J 2014 *Nat. Mater.* **13** 11
[4] Sharad M, Augustine C, Panagopoulos G and Roy K 2012 *IEEE Trans. Nanotechnol.* **11** 843–53
[5] Yamada K, Murayama S and Nakatani Y 2016 *Appl. Phys. Lett.* **108** 202405
[6] Schellekens A J, van den Brink A, Franken J H, Swagten H J M and Koopmans B 2012 *Nat. Commun.* **3** 847
[7] Lin W, Vernier N, Agnus G, Garcia K, Ocker B, Zhao W, Fullerton E E and Ravelosona D 2016 *Nat. Commun.* **7** 13532
[8] Ando F, Kakizakai H, Koyama T, Yamada K, Kawaguchi M, Kim S, Kim K-J, Moriyama T, Chiba D and Ono T 2016 *Appl. Phys. Lett.* **109** 022401
[9] Chiba D, Kawaguchi M, Fukami S, Ishiwata N, Shimamura K, Kobayashi K and Ono T 2012 *Nat. Commun.* **3** 888
[10] Bauer U, Emori S and Beach G S D 2012 *Appl. Phys. Lett.* **101** 172402
[11] Ma C, Zhang X, Xia J, Ezawa M, Jiang W, Ono T, Piramanayagam S N, Morisako A, Zhou Y and Liu X 2019 *Nano. Lett.* **19** 353
[12] Tan F N, Gan W L, Ang C C I, Wong G D H, Liu H X, Poh F and Lew W S 2019 *Sci. Rep.* **9** 7369
[13] Yang S H, Ryu K S and Parkin S 2015 *Nat. Nanotechnol.* **10** 221
[14] Yu Z, Zhang Y, Zhang Z, Cheng M, Lu X, Yang Z, Shi J and Xiong R 2018 *Nanotechnology* **29** 175404
[15] Ang C C I, Gan W and Lew W S 2019 *New J. Phys.* **21** 043006
[16] Zhang Y, Luo S, Yang X and Yang C 2017 *Sci. Rep.* **7** 2047
[17] Rohart S and Thiaville A 2013 *Phys. Rev.* B **88** 184422
[18] Sampaio J, Cros V, Rohart S, Thiaville A and Fert A 2013 *Nat. Nanotechnol.* **8** 839

[19] Iihama S, Ma Q, Kubota T, Mizukami S, Ando Y and Miyazaki T 2012 *Appl. Phys. Express* **5** 083001
[20] Emori S, Bauer U, Ahn S-M, Martinez E and Beach G S D 2013 *Nat. Mater.* **12** 611
[21] Boulle O, Rohart S, Buda-Prejbeanu L D, Jué E, Miron I M, Pizzini S, Vogel J, Gaudin G and Thiaville A 2013 *Phys. Rev. Lett.* **111** 217203
[22] Martinez E, Emori S, Perez N, Torres L and Beach G S D 2014 *J. Appl. Phys.* **115** 213909
[23] Ryu K-S, Thomas L, Yang S-H and Parkin S S P 2012 *Appl. Phys. Express* **5** 093006
[24] Shen M, Zhang Y, Luo W, You L and Yang X 2019 *J. Magn. Magn. Mater.* **485** 69
[25] Yang S H and Parkin S 2017 *J. Phys. Condens. Matter* **29** 303001
[26] Shen M, Zhang Y, You L and Yang X 2018 *Appl. Phys. Lett.* **113** 152401
[27] Thiaville A, Rohart S, Jué É, Cros V and Fert A 2012 *Europhys. Lett.* **100** 57002
[28] Rana B and Otani Y 2018 *Phys. Rev. Appl.* **9** 014033
[29] Liu M, Obi O, Cai Z, Lou J, Yang G, Ziemer K S and Sun N X 2010 *J. Appl. Phys.* **107** 073916
[30] Liu M *et al* 2009 *Adv. Funct. Mater.* **19** 1826
[31] Wang W G, Li M, Hagemen S and Chien C L 2012 *Nat. Mater.* **11** 64